East European Journal of Physics. 3. 223-232 (2025)
DOI:10.26565/2312-4334-2025-3-19 ISSN 2312-4334

IMPACT OF COMBINED CHEMICAL REACTIONS AND THERMAL DISPERSION ON CONVECTIVE FLOW IN HYBRID NANOFLUID POROUS MEDIUM

Zohra Terbiche[a], Hamza Ali Agha[a,b]*, Soufiane Rahal[a], Nadir Boutalbi[b]
[a]*Biomaterials and Transport Phenomena Laboratory (LBMPT), Faculty of technology, University Yahia Fares of Medea, Pole Urbain Medea, 26000, Algeria*
[b]*Mechanic, Materials and Energetic Laboratory (L2ME), Faculty of technology, University A. MIRA of Bejaia, Targua Ouzmour Bejaia, 06000, Algeria*
**Corresponding author: aliagha.hamza@univ-medea.dz*
Received May 1, 2025; revised May 26, 2025; in final form June 12, 2025; accepted June 19, 2026

The present study is characterized by numerical analysis concerning thermal dispersion's influence on heat and mass transfer flow towards a stretching plate in a saturated porous medium filled with Cu/Al_2O_3-water hybrid nanofluid, considering the presence of homogeneous (HOM)-heterogeneous (HET) chemical reactions. A new model of (HOM-HET) chemical reactions is constructed where the (HET) reactions occur on the surfaces of the solid matrix within the porous medium and the plate, following first-order kinetics. In contrast, the homogeneous (HOM) reaction takes place in the fluid phase and is described by isothermal cubic autocatalytic kinetics. The momentum, energy, and mass transfer phenomena are governed by a set of partial differential equations with appropriate similarity transformations that yield four coupled nonlinear ordinary differential equations. The resulting system of governing equations is solved numerically through a computationally efficient finite-difference scheme. The numerical results are validated through comparison with available data, showing good agreement. The numerical results demonstrate the influence of physical control parameters on the flow dynamics, thermal distribution, and solute concentration profiles. Furthermore, key solution characteristics, including the Nusselt number and skin friction coefficient, are tabulated.
Keywords: *Hybrid nanofluid; Thermal dispersion; Stagnation-point flow; Porous medium*
PACS: 47.11.-j, 63.20.D, 47.55.P, 44.30.+v

Nomenclature

A, B	Chemical species	K_c	Homogeneous reaction parameter
D_A, D_B	Diffusion coefficients of species A and B, respectively	K_s	Heterogeneous reaction parameter
a, b	Concentration of chemical species A and B, respectively	K_{sv}	Surface-catalyzed parameter
a_0, b_0	Initial concentration of species A and B, respectively	Sc	Schmidt number
c_p	Specific heat at constant temperature	Nu_x	Local Nusselt number
d	Mean particle diameter	Pr	Prandtl number
G, H	Dimensionless concentrations of chemical species A and B	Re_x	Reynolds number
K	Permeability of the porous medium	S	Interfacial area
K_1	Parameter of the porous medium	T	Fluid temperature
k_c	Reaction rate constant of homogeneous reaction	T_∞	Ambient temperature attained as y tends to infinity
k_s	Reaction rate constant of homogeneous reaction	U_w	Stretching sheet velocity
k_{hnf}	Thermal conductivity of hybrid nanofluid	U_∞	Free stream velocity
k_f	Thermal conductivity of pure water	u,v	Velocity components in the x and y directions
k_{s1}	Thermal conductivity of copper nanoparticle	x,y	Cartesian coordinates
k_{s2}	Thermal conductivity of alumina nanoparticle		

Greek symbols

		ν_{hnf}	Kinematic viscosity of hybrid fluid
α_d	Dispersion diffusivity	ν_f	Kinematic viscosity of base fluid
α_{eff}	Effective thermal diffusivity	θ	Dimensionless temperature
α_{hnf}	Molecular diffusivity of nanofluid	ρ	Density
γ	Dispersion coefficient of the porous medium	ψ	Stream function.
η	Similarity variable	δ	Ratio of the diffusion coefficient
λ	Positive constant	ε	Velocity ratio parameter
μ_{hnf}	Dynamic viscosity of the hybrid nanofluid		

INTRODUCTION

The interaction between nanofluid flow and heat/mass transfer through a porous medium is a multifaceted process governed by intricate fluid dynamics as well as thermal and mass transfer phenomena. The presence of nanoparticles such as metals, carbides, oxides, or carbon nanotubes in a base fluid such as water, ethylene glycol, oil, or toluene can affect the flow behavior, leading to changes in heat and mass transfer rates and patterns by increasing the thermal properties of the base fluid. Analysing heat and mass transfer characteristics in porous media filled with nanofluid is crucial for various engineering applications including heat exchangers, thermal management systems, enhanced energy recovery, geothermal energy extraction, and chemical engineering. Advanced computational modeling and experimental studies are employed

Cite as: Z. Terbiche, H.Ali Agha, S. Rahal, N. Boutalbi, East Eur. J. Phys. 3, 223 (2025), https://doi.org/10.26565/2312-4334-2025-3-19

to analyze and optimize these processes for improved efficiency and performance in practical applications. Comprehensive reviews on nanofluid-saturated porous media have been conducted by Khanafer and Vafai [1], Vafai and coworkers [2,3], and by Nield and Bejan [4].

In addition, the convective flow of a nanofluid through a porous medium over stretching objects is widely studied by several researchers because of the importance of this phenomenon, which is prevalent in various engineering and environmental applications. In this context, Sowmiya and Kumar [5] discussed numerically the influence of magnetic field and thermal radiation in porous medium filled with Williamson nanofluid within a stretching cylinder. The objective of this study was to investegate the impact of rheological characteristics on flow behavior in a cylinder geometry. Khalil et al. [6] studied numerically (Fe_3O_4-Cu) hybrid nanofluid flow in a porous medium over an exponentially stretching plate in presence of Joule heating and thermal radiation. Dulal Pal and Mandal [7] presented the effects of thermal radiation on mixed convection towards a stagnation-point flow over a moving plate in a porous medium with heat generation and viscous dissipation. This study revealed that the suction parameter reduces the dynamic behavior and temperature profiles in the stretching-sheet situation, whereas the opposite tendency arises in the shrinking-sheet case. Adigun et al. [8] discussed the magnetohydrodynamic (MHD) stagnation-point flow of a viscoelastic nanofluid past an inclined cylinder stretching linearly. Nandi et al. [9] explored the impact of nonlinear thermal radiation and heat generation on MHD stagnation point flow of nanofluid containing Fe_3O_4, Cu and Ag nanoparticles along a permeable stretching plate embedded in a porous medium. Asogwa et al. [10] examined the external thermal radiation effects on electromagnetohydrodynamic (EMHD) boundary layer flow of non-Newtonian nanofluid over reactive stretching surface, considering combined thermal transport properties. They found that the control parameters play an important role in modification of the dynamic, heat and mass behaviors.

Another level of complexity emerges in flow within porous media when dispersion mechanisms are taken into account. This complexity can manifest as significant thermal dispersion, wherein heat undergoes molecular diffusion as a result of mixing and recirculation of local fluid currents induced by the complicated flow paths through the porous medium. In this context, Kameswaran and Sibanda [11] investigate numerically via the shooting technique the effects of thermal dispersion on non-Newtonian power-law nanofluid flow over an impermeable vertical plate. From this work, the results reveal that under a constant thermal dispersion parameter, the thermal boundary layer thickness reduces with increasing power-law index values, a trend consistent in both aiding and opposing buoyancy situations. Bouaziz and Hanini [12] mainly explore thermal and solute dispersions in the simultaneous heat and mass transfer along a vertical plate immersed into a non-Darcy saturated porous medium with a Buongiorno nanofluid. Sheremet et al. [13] studied the effect of thermal dispersion on transient natural convection in a wavy-walled porous cavity using the Tiwari and Das nanofluid model. A numerical analysis was achieved by RamReddy and Venkata [14] to study the combined effects of double dispersion and the convective boundary condition on natural convection flow over vertical frustum of a cone in a nanofluid saturated non-Darcy porous medium. They take into account the Brownian motion and thermophoresis mechanisms. Sudhagar et al. [15] studied the impact of thermal dispersion on the mixed convective boundary layer nanofluid flow past over an isothermal vertical wedge implanted in a porous medium. They observed that the presence of thermal dispersion could affect fluid flow and temperature profiles. Awad et al. [16] investigate free convection nanofluid flow in a porous layer with double dispersion effects. They have use the Forchheimer extension for porous medium and Buongiorno nanofluid, which incorporates Brownian motion and thermophoresis parameters. Meena et al. [17] investigate mixed convection flow over a vertical cone in a saturated porous medium with the presence of thermal and solutal dispersion effects. Khashi'ie et al. [18] numerically analyze the mixed convection flow of Cu-Al_2O_3/water nanofluid along a vertical plate embedded in a porous medium under the presence of thermal dispersion. They take into consideration the assisting and opposing flows, and they found that in the opposing buoyancy region, dual solutions are expected, and the presence of nanoparticles and thermal dispersion can modify the dynamic and thermal behavior in the boundary layers.

Furthermore, chemically reactive flows in porous media have received increasing interest over the last three decades. The combined impact of homogeneous and heterogeneous reactions pertains to scenarios where both categories of reactions take occur simultaneously within a chemical or physical system. Homogeneous reactions take place in a single phase, typically the gas or liquid phase, while heterogeneous reactions involve interfaces between different phases, such as gas-solid or liquid-solid reactions. Understanding the interaction between these reactions is essential in various fields, including chemistry, chemical engineering, combustion and catalysis. The reactive transport is usually described by partial differential equations [19]. The first model describing the isothermal homogeneous–heterogeneous reactions in boundary layer flow of a viscous fluid was developed by Chaudhary and Merkin [20,21]. In this area of interest, Alzahrani et al. [22] investigate the thermal evaluation of viscoelastic nanofluid flow past a porous surface with a heat source/sink and the presence of homogeneous and heterogeneous reactions. They found that for higher values of homogeneous and heterogeneous reaction parameters, mass transfer is greater in fluid flow with aggregation conditions. Liu et al. [23] discussed the impact of catalytic homogeneous-heterogeneous reactions in a Darcy porous medium. They found that an increase in the interfacial area of porous media enhances the rate of surface-catalyzed reactions, thereby significantly shortening chemical reaction time. The influence of induced magnetic field on Darcy–Forchheimer nanofluid flows comprising carbon nanotubes with homogeneous-heterogeneous reactions was performed by Bashir et al. [24]. The goal of this study is to conduct a comparative analysis of Darcy–Forchheimer nanofluid flows containing CNTs of both multi-wall (MWCNTs) and single-wall carbon nanotubes (SWCNTs) immersed in two different base fluids over a stretched

surface. Irfan et al. [25] examined the interplay of coupled homogeneous-heterogeneous reactions and non-Fourier heat flux (Cattaneo-Christov model) in a non-Newtonian fluid with variable thermal conductivity. Their analysis revealed that the thermal relaxation parameter significantly modulates the temperature distribution, whereas the concentration profile demonstrates an inverse correlation between the Schmidt number and the homogeneous reaction parameter. The influence of nanoparticle aggregation on heat transfer phenomena of second grade nanofluid flow over melting surface subject to homogeneous-heterogeneous reactions was investigated by Sunthrayuth et al. [26]. They showed that higher mass transfer for fluid flow with aggregation condition is observed for increased values of heterogeneous and homogeneous reaction parameters. Abbas and Sheikh [27] studied numerically the stagnation point flow of ferrofluid over a flat plate with non-linear slip boundary condition in the presence of homogeneous–heterogeneous reactions. Hayat et al. [28] studied the phenomenon of melting heat transfer in the presence of homogeneous-heterogeneous reactions and a magnetic field in flow along a stretching surface with variable thickness.

In view of all the above-mentioned applications and from the literature context of study, it is observed that hybrid nanofluid reactive flow over a porous stretchable sheet in the presence of thermal dispersion has not yet been investigated. The purpose of the current paper is to emphasize the effects of thermal dispersion on Darcy convection boundary layer flow over a stretching plate in the presence of coupled homogeneous-heterogeneous reactions (H-H-R). Cu/Al_2O_3 hybrid nanoparticles are used in the base fluid. The behavior of different profiles has been examined and displayed graphically. Moreover, the interesting features of the solutions in terms of the number of Nusselt and skin friction coefficient are calculated.

PROBLEM STATEMENT

Consider a two-dimensional steady boundary layer flow over a stretching sheet in a laminar and incompressible nanoliquid of constant ambient temperature T_∞. In this study, a water-based nanofluid containing two types of nanoparticles Cu /Al_2O_3 is used as working fluid. The nanoparticles are assumed to have a uniform shape and size. Figure 1 describes the physical model and the coordinate system, where the x and y axes are measured along the surface of the sheet and normal to it, respectively. The stretching velocity $U_w(x)$ and the ambient fluid velocity, $U_\infty(x)$, is assumed to increase linearly from the stagnation point, i.e., $U_w(x) = \lambda x$ and $U_w(x) = cx$, where λ and c are constant with c > 0. We note that λ > 0 correspond to stretching sheet.

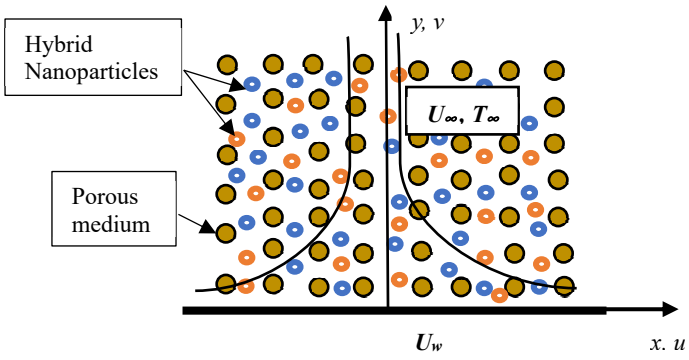

Figure 1. Physical Sketch of the model

It is supposed that the temperature at the surface, T_w, varies along the sheet and changes with position x. Additionally, the base fluid and nanoparticles are in thermal equilibrium, with no slip occurring between them.

The Darcy model is used to describe the reactive flow in porous medium, which contains a reactive species (A) that reacts to form some product (B) when in contact with the plate surface. In particular, the following two types of reactions are applied:

- An isothermal cubic autocatalytic reaction which takes place in the porous medium, this reaction is given schematically by $A + 2B \rightarrow 3B$, $rate = k_c ab^2$.
- A single first-order exothermic catalytic reaction on the plate surface whereby reactant (A) is converted to a product (B); $A \rightarrow B$, $rate = k_s a$

These two basic models are widely used by several researchers, for more details, see [20, 25].
Notably, the porous medium and stretching surface share the same catalytic material, enabling heterogeneous reactions to occur on the solid matrix of the porous medium. These surface-catalyzed reactions are governed by the kinetic model outlined in [23] $r_p = -Sk_s$.

The boundary layer equations, incorporating the momentum, energy, and mass equations, can be expressed in dimensional form as follows, according to the previously stated assumptions:

$$\frac{\partial u}{\partial x} + \frac{\partial v}{\partial y} = 0, \tag{1}$$

$$u\frac{\partial u}{\partial x}+v\frac{\partial u}{\partial y}=U_{\infty}\frac{dU_{\infty}}{dx}+\frac{\mu_{hnf}}{\rho_{hnf}}\frac{\partial^2 u}{\partial y^2}+\frac{\mu_{hnf}}{\rho_{hnf}K}\left(U_{\infty}(x)-u\right), \tag{2}$$

$$u\frac{\partial T}{\partial x}+v\frac{\partial T}{\partial y}=\frac{\partial}{\partial y}\left(\alpha_{eff}\frac{\partial T}{\partial y}\right), \tag{3}$$

$$u\frac{\partial a}{\partial x}+v\frac{\partial a}{\partial y}=D_A\frac{\partial^2 a}{\partial y^2}-k_c ab^2-Sk_s a\,, \tag{4}$$

$$u\frac{\partial b}{\partial x}+v\frac{\partial b}{\partial y}=D_B\frac{\partial^2 b}{\partial y^2}+k_c ab^2+Sk_s a\,. \tag{5}$$

Here x and y are distances along and perpendicular to the surface, u and v are the velocity components in the x and y directions, respectively. T is the temperature, K is permeability of porous medium, μ_{hnf} is the viscosity of the hybrid nanofluid, ρ_{hnf} is the density of the hybrid nanofluid, α_{eff} characterize the effective thermal diffusivity which is the sum of the molecular diffusivity α_{hnf} of hybrid nanofluid and the dispersion diffusivity α_d, where $\alpha_d=\gamma ud$. Here γ is the thermal dispersion coefficient, u is stream-wise velocity and d denotes to the mean particle diameter. Note that, this model is valid for fluids and nanofluids as mentioned in [12, 18, 29, 30 and 31]. (D_A, D_B) the diffusion species coefficients of reactant (A) and product (B), (a, b) are the concentration of chemical species of (A) and (B), respectively. k_c and k_s denote the rate constants of homogeneous and heterogeneous reactions, respectively. S is the interfacial area of the porous media.

The correlations of the hybrid nanofluid are presented in Table 1, where s_1 and s_2 denotes the copper and alumina nanoparticles, respectively, ϕ_1 and ϕ_2 are the volumetric concentration of Cu and Al_2O_3 nanoparticles, accordingly. In addition, the subscript f denotes the base fluid. In Table 1, $\phi_{hnf}=\phi_1+\phi_2$ where $\phi_{hnf}=0$ corresponds to a regular fluid (pure water). The thermophysical properties of the water and respective nanoparticles are detailed in Table 2.

The boundary conditions associated with the above problem are as follows:

$$u=U_w(x)=\lambda x;\ \mathrm{v}=0;\ \mathrm{T_w}=T_{\infty}+w\left(\frac{x}{l}\right)^2;\ \mathrm{D_a}\frac{\partial a}{\partial y}=-D_B\frac{\partial b}{\partial y}=k_s a;\quad \text{as y}=0\,, \tag{6}$$

$$u=U_{\infty}(x)=cx;\ \mathrm{T}\to T_{\infty};\ a\to \mathrm{a}_0;\ \mathrm{b}\to 0\qquad \text{as y}\to\infty\,. \tag{7}$$

Table 1. The correlations of hybrid nanofluids (see Babu et al. [32] and Takabi and Salehi 33]).

Properties	Nanofluids
Density (ρ)	$\rho_{hnf}=(1-\varphi_{hnf})\rho_f+\varphi_1\rho_{s1}+\varphi_2\rho_{s2}$
Capacity Heat (ρc_p)	$(\rho c_p)_{hnf}=(1-\varphi_{hnf})(\rho c_p)_f+\varphi_1(\rho c_p)_{s1}+\varphi_2(\rho c_p)_{s2}$
Dynamic Viscocity (μ)	$\mu_{hnf}=\dfrac{\mu_f}{(1-\varphi_{hnf})^{2.5}}$
Thermal Conductivity (k)	$\dfrac{k_{hnf}}{k_f}=\left[\dfrac{\left(\frac{\varphi_1 k_{s1}+\varphi_2 k_{s2}}{\varphi_{hnf}}\right)+2k_f+2(\varphi_1 k_{s1}+\varphi_2 k_{s2})-2\varphi_{hnf}k_f}{\left(\frac{\varphi_1 k_{s1}+\varphi_2 k_{s2}}{\varphi_{hnf}}\right)+2k_f-(\varphi_1 k_{s1}+\varphi_2 k_{s2})+\varphi_{hnf}k_f}\right]$

Table 2. Thermophysical properties of water and nanoparticles (Oztop and Abu-Nada [34]).

Physical properties	Water	Cu	Al_2O_3
c_p (J/kg K)	4179	385	765
ρ (kg/m^3)	997.1	8933	3970
k(W/m.K)	0.613	400	40

The governing Eqs. (1-5) subject to the boundary conditions (6-7) can be expressed in a nondimensional form by introducing the following transformations [38] and [39]:

$$\eta=\left(\frac{c}{\nu_f}\right)^{\frac{1}{2}}y\,;\ \psi=(\nu_f c)^{\frac{1}{2}}xf(\eta)\,;\ \theta(\eta)=\frac{T-T_{\infty}}{T_w-T_{\infty}}\,;\ G=\frac{a}{a_0}\,;\ H=\frac{b}{a_0}$$

G and H are dimensionless concentrations of species (A) and (B), respectively.

ψ is the stream function defined as $u = \frac{\partial \psi}{\partial y};\ v = -\frac{\partial \psi}{\partial x}$.

Equations (1– 5) can be reduced to a set of ordinary differential equations by applying the similarity variables defined above.

$$f''' + K_1\left(1 - f'\right) + A_1\left(1 + ff'' - f'^2\right) = 0 \tag{8}$$

$$\frac{k_{hnf}/k_f}{A_2}\theta'' + Ds\left(f'\theta'\right)' + \Pr\left(f\theta' - 2f'\theta\right) = 0 \tag{9}$$

$$\frac{1}{Sc}G'' - K_c GH^2 - K_{sv}G + fG' = 0 \tag{10}$$

$$\frac{\delta}{Sc}H'' + K_c GH^2 + K_{sv}G + fH' = 0 \tag{11}$$

Building on the work of Chaudhary and Merkin [20, 21], we consider a common practical situation where the diffusion coefficients D_A and D_B for chemical species (A) and (B) are of similar magnitude and size. Consequently, we assume $D_A = D_B$, leading to δ=1. Under this assumption, the following relation is obtained:

$$G(\eta) + H(\eta) = 1 \tag{12}$$

Equations (10) and (11) under this assumption reduce to:

$$\frac{1}{Sc}G'' - K_c G\left(1 - G\right)^2 - K_{sv}G + fG' = 0 \tag{13}$$

Given the boundary conditions (6 –7), which are now written as:

$$f = 0;\ \mathrm{f}' = \varepsilon;\ \theta = 1;\ \mathrm{G}' = \mathrm{K_s}G;\ \ \delta\mathrm{H}' = \mathrm{K_s}G \quad \text{as } \eta = 0 \tag{14}$$

$$\mathrm{f}' \to 1;\ \theta \to 0;\ \mathrm{G} \to 1\ \ \mathrm{H} \to 0 \quad \text{as } \eta \to \infty. \tag{15}$$

In the equations above, K_1 porous medium parameter, Thermal dispersion parameter, Prandtl number, ε is the velocity ratio parameter, K_c, K_s are the homogeneous and heterogeneous reaction parameter, respectively. K_{sv} represent the surface-catalyzed parameter, δ is the ratio of diffusion coefficients, the Schmidt number Sc.

$$K_1 = \frac{\nu_f}{Kc};\ Ds = \frac{\gamma d U_\infty}{\alpha_f};\ \Pr = \frac{\nu_f}{\alpha_f};\ \varepsilon = \frac{c}{\lambda};\ K_c = \frac{k_c a_0^2}{c};\ K_s = \left(\frac{\nu_f}{c}\right)^{\frac{1}{2}}\frac{k_s}{D_A};\ K_{sv} = S_v K_s;\ Sc = \frac{\nu_f}{D_A}\ S_v = \frac{SD_A}{(c\nu)^{\frac{1}{2}}},\ \delta = \frac{D_B}{D_A},$$

$$A_1 = \left(1 - \varphi_{hnf}\right)^{2.5}\left(\left(1 - \varphi_{hnf}\right) + \varphi_1\frac{\rho_{s1}}{\rho_f} + \varphi_2\frac{\rho_{s2}}{\rho_f}\right),\ A_2 = \left(\left(1 - \varphi_{hnf}\right) + \varphi_1\frac{\left(\rho c_p\right)_{s1}}{\left(\rho c_p\right)_f} + \varphi_2\frac{\left(\rho c_p\right)_{s2}}{\left(\rho c_p\right)_f}\right)$$

The physical quantities of interest are the skin friction coefficient C_f and the local Nusselt number Nux, which are defined as:

$$C_f = \frac{\mu_{hnf}}{\rho_f U_\infty^2}\left(\frac{\partial u}{\partial y}\right)_{y=0};\quad Nu_x = \frac{xk_{hnf}}{k_f\left(T_w - T_\infty\right)}\left(-\frac{\partial T}{\partial y}\right)_{y=0}$$

With μ_{hnf} and k_{hnf} being the dynamic viscosity and thermal conductivity of the nanofluids, respectively. Applying the similarity transformations, we obtain:

$$\mathrm{Re}_x^{1/2}\,C_f = \frac{1}{\left(1 - \varphi_{hnf}\right)^{2.5}}f''(0) \tag{16}$$

$$\mathrm{Re}_x^{-1/2}\,Nu_x = -\frac{k_{hnf}}{k_f}\theta'(0) \tag{17}$$

RESULTS AND DISCUSSIONS

The governing ordinary differential equations (8, 9, and 13), along with the boundary conditions (14–15), were numerically solved using the finite difference scheme implemented through the bvp4c package in Matlab. This package

utilizes the three-stage Lobatto collocation formula, ensuring a continuous solution with fourth-order accuracy. Mesh selection and error control are determined based on the residual of the continuous solution. This method has proven successful in numerous research endeavors as [35] and [36]. For further insights, refer to [37].

In order to verify the accuracy of our present technique, we have compared obtained numerical solutions, through the skin friction coefficient and local Nusselt number for the case where the stretched surface is isothermal and without thermal dispersion effects. From the table 3, it is seen that the present results are in excellent agreement with both results presented by Bachok [38], Nandkeolyar et al. [39] and Yacob et al. [40].

Table 3. Values of $\mathrm{Re}_x^{-1/2} Nu_x$ and $\mathrm{Re}_x^{1/2} C_f$ for some values of ϕ_1, ϕ_2 and ε

		(Cu-water)					
		Bachok [38].		Nandkeolyar et al. [39].		Present work	
ε	ϕ_1	$Rex^{1/2}Cf$	$Nu_xRex^{-1/2}$	$Rex^{1/2}Cf$	$Nu_xRex^{-1/2}$	$Rex^{1/2}Cf$	$Nu_xRex^{-1/2}$
0	0.1	1.8843	1.4043	1.8832	1.404329	1.884323	1.404327
	0.2	2.6226	1.6692	2.6227	1.669343	2.622743	1.669337
0.5	0.1	1.0904	1.8724	1.0904	1.872389	1.090452	1.872386
	0.2	1.5177	2.1377	1.5177	2.157696	1.517773	2.157690
		(Al_2O_3-water)					
		Bachok [38].		Yacob et al. [40].		Present work	
ε	ϕ_2	$Rex^{1/2}Cf$	$Nu_xRex^{-1/2}$	$Rex^{1/2}Cf$	$Nu_xRex^{-1/2}$	$Rex^{1/2}Cf$	$Nu_xRex^{-1/2}$
0	0.1	1.6019	1.3305	1.6019	1.3305	1.6020	1.3305
	0.2	2.0584	1.5352	2.0584	1.5352	2.0584	1.5352
0.5	0.1	0.9271	1.8278	-	-	0.9270	1.8279
	0.2	1.1912	2.0700	-	-	1.1912	2.0700

The parametric study results reported in this section are displayed using graphical illustrations to highlight the effect of several parameters such as K_1, Ds, K_c, K_{sv}, K_s ϕ_1, ϕ_2 as well as stretching parameter ε on velocity, temperature, and concentration. Numerical computations are done for $0.5 \le K_1 \le 4.0$; $0.0 \le Ds \le 3.0$; $0.05 \le \phi_1, \phi_2 \le 0.09$; $0.5 \le K_c \le 1.5$; $0.0 \le K_s \le 5$; $0.1 \le K_{sv} \le 0.5$; $0.5 \le \varepsilon \le 4.0$.

The variation of non-dimensional velocity distribution against the similarity variable η is shown respectively in Figure 2 for a few sets of values of ε and K_1.

Figure 2 depicts the dynamic behavior of axial velocity for different values of K_1 and ε. The curves corresponding to various values of ε exhibit a slight vertical shift for a given K_1. From this figure, as the porous medium parameter increases, the velocity decreases and consequently the dynamic boundary layer becomes thicker. This effect physically is due to the enhanced resistance imposed by the porous medium in term of permeability on the fluid flow. Additionally, the presence of nanoparticles in a nanofluid can also influence flow through porous media, potentially leading to changes in permeability due to particle interactions with the pore walls or the formation of particle bridges. The same tendency was observed by Kameswaran et al. [41] for single nanoparticles (Al_2O_3 / water) nanofluids. Furthermore, a higher stretching parameter promotes faster flow and results in a larger momentum boundary layer.

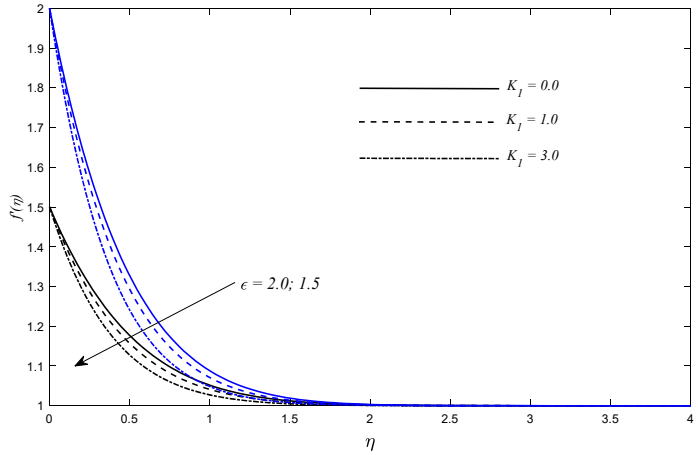

Figure 2. Variation of velocity profiles with η, for varying ε and K_1
(Ds = 1.0, Pr = 6.2, Kc = Ks = 0.5, Sc = 1.0, Ksv = 0.1, $\phi_1 = \phi_2 = 0.02$)

The temperature distributions against the space variable η are demonstrated in Figure 3 for some values of thermal dispersion Ds and stretching parameter ε. A notable observation from this figure is that the temperature profiles gradually

approach zero as the distance from the boundary increases, ensuring compliance with the boundary conditions. An analysis of this figure reveals that the temperature profiles increase in direct proportion to the thermal dispersion parameter. In addition, the increasing in thermal dispersion term leads to enhance the thermal boundary layer thickness. These outcomes are subjectively like those got by Sudhagar et al. [15] on account of a Buongiorno nanofluid. The effect of thermal dispersion increases the temperature, bringing about surpassing flow rates at the surface. This is in agreement with the expected physical behavior. Besides, the augmentation in stretching parameter leads to reduction in the dimensionless temperature.

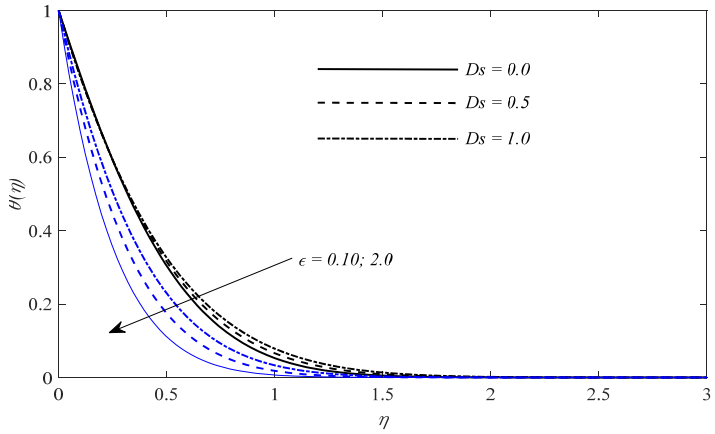

Figure 3. Variation of temperature profiles with η, for varying ε and *Ds*

(K1=1.0; Kc = Ks = 0.5, Sc=1.0, Ksv=0.1, $\phi_1=\phi_2=0.1$)

The numerical results for the mass transport of chemical species (A) are presented in Figures 4-6 for different values of some governing parameters, namely K_c, K_{sv} and K_s. Figure 4 represents the effects of the parameter surface-catalyzed K_{vs} and homogeneous reaction parameters K_c on the dimensionless concentration $G(\eta)$. The numerical results show that an improvement in K_{sv} and K_c reduces the concentration, causing the mass boundary layer becomes to thicken. Physically, when the reaction interface on solid matrix of the porous medium augment, the catalyzed reaction accelerates and the concentration of species (A) reaches its lowest a fixed position η gradually. Liu et al. observed the similar results for Al_2O_3-water nanofluid (see [23]). The impact of both the stretching parameter and the heterogeneous reaction parameter is displayed in Figure 5.

From this figure, it is observed that for $\varepsilon = 0.1$ the concentration of the species (A) is lower compared to the concentration when $\varepsilon = 3.0$ at ($\eta = 0$) which means that when the stretching velocity is slow, the reaction on the sheet becomes faster. In addition, the augmentation in K_s promotes the catalytic reaction at the surface of the sheet. Consequently, the mass transfer becomes more important, and the boundary layer becomes thicker. Figure 6 illustrates the influence of the combined effect of K_c, K_{sv}, and K_s on the decay of the concentration profile when the spatial variable (η) is equal to zero. It is observed that an increase in homogeneous and heterogeneous reaction parameters leads to a decrease in the concentration of species and the mass transfer rate to the plate. Furthermore, it is observed that the concentration at the surface decreases as the strength of the HOM-HET reactions increases. It is worth noting that the surface catalytic parameter has a significant influence on the surface concentration. The intense surface catalytic reaction on porous media leads to a lower wall concentration.

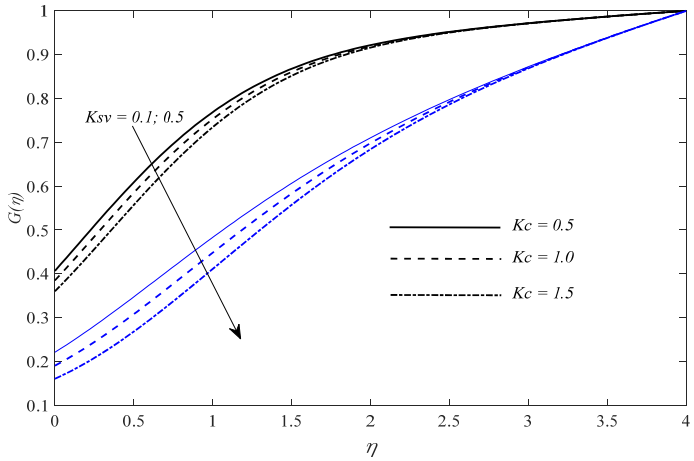

Figure 4. Effect of Ksv and Kc on the concentration profiles.
(K1 = 1.0, Ds = 1.0, Pr = 6.2, Sc = 1.0, $\phi1=\phi2=0.05$).

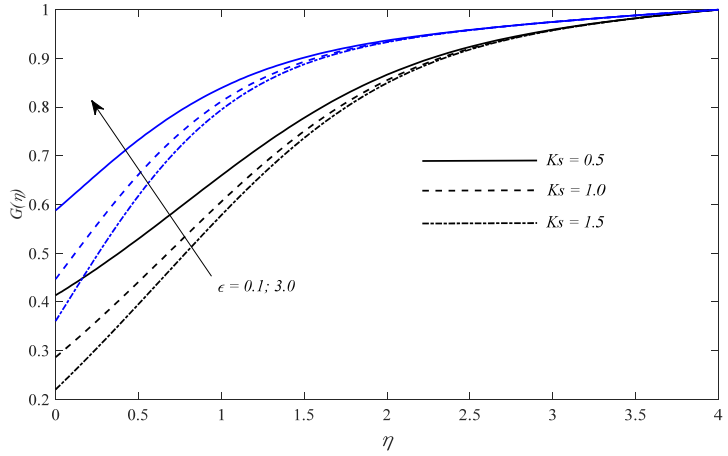

Figure 5. Effect of Ks and $\boldsymbol{\varepsilon}$ on the concentration profiles.
(K_1 = 1.0, Ds = 1.0, Pr = 6.2, Kc = 0.5, Sc = 1.0, Ksv = 0.1, $\phi_1 = \phi_2$ = 0.05).

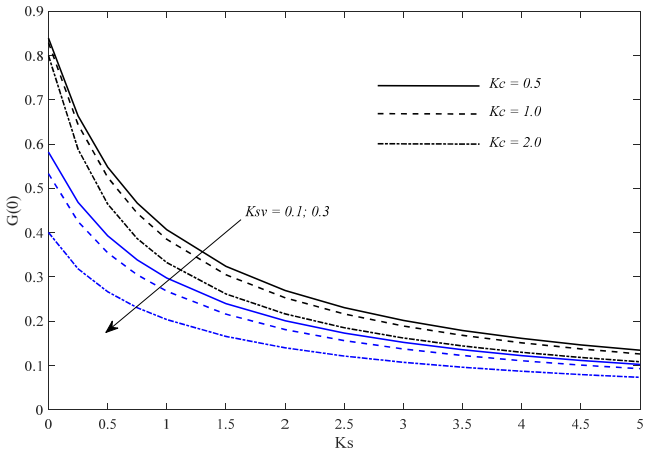

Figure 6. Effect of *K*sv, *K*c and *K*s on the concentration profiles G (0)
(K_1 = 1.0, Ds = 1.0, Pr = 6.2, Sc =1.0, $\phi_1 = \phi_2$ = 0.05; ε = 2)

The effects of increase in the values of ε, ϕ_1, ϕ_2, K_1, and Ds on the skin friction, which is proportional $f''(0)$, and the Nusselt number which measures the rate of heat transfer at the plate and can be measured as a variation in $\theta''(0)$ as mentioned in Eqs (16 and 17). Some values of these interest quantities are calculated in Table 4.

Table 4. Values of $\mathrm{Re}_x^{-1/2} Nu_x$ and $\mathrm{Re}_x^{1/2} C_f$ for selected values of parameters. $K_c = K_s = 1.0$, $K_{sv} = 0.10$, $Sc = 0.5$.

ε	$\phi_1 = \phi_2$	K_1	Ds	$\mathrm{Re}_x^{1/2} C_f$	$\mathrm{Re}_x^{-1/2} Nu_x$
0.5	0.05	1.0	1.0	0.6507	1.7270
1.5	-	-	-	-0.6507	1.7040
2.0	-	-	-	-1.3013	1.6835
4.0	-	-	-	-3.9040	1.5925
2	0.01	1.0	1.0	-2.2333	1.4151
-	0.05	-	-	-2.5974	1.6835
-	0.07	-	-	-2.7600	1.8294
-	0.09	-	-	-2.9116	1.9841
2	0.05	0.5	1.0	-2.4716	1.6936
-	-	1.0	-	-2.5974	1.6835
-	-	2.0	-	-2.8331	1.6654
-	-	4.0	-	-3.2551	1.6359
2	0.05	1.0	0.0	-2.5874	2.9281
-	-	-	0.5	-2.5874	2.0904
-	-	-	1.0	-2.5874	1.6835
-	-	-	3.0	-2.5874	1.0403

It can be seen the augmentation in the stretching parameter and volume fraction of the hybrid of nanoparticles leads to enhance the heat exchange between the surface of plate and the fluid on porous medium. This augmentation is due to

presence of nanoparticles, which include a higher thermal conductivity as compared with clear nanofluid ($\phi_1 = \phi_2 = 0$). On the other hand, when the thermal dispersion and porous medium parameter rise up the heat transfer rate decrease. Regarding the skin friction coefficient, it can be observed that the presence on nanoparticles can ameliorate the skin friction. Whereas, the stretching velocity speed up the friction coefficient decrease. The same tendency observed for porous medium parameter. Physically, this effect is due to the presence of hybrid nanoparticles, which gives a higher drag force in opposition to the flow in porous medium.

CONCLUDING REMARKS

In this work, we studied the impact of thermal dispersion under the presence of coupled homogeneous-heterogeneous reactions on a convective flow through a porous medium filled by hybrid nanofluid. Copper (Cu) and aluminum oxide (Al_2O_3) were taken as nanoparticles and water as the base fluid. We used the Darcy model in the momentum equation and we supposed non-uniform boundary conditions in term of temperature and velocity. The partial differential equations are converted into ordinary differential equations applying appropriate similarity transformations. Validated by some results shown in the literature. The important results of this parametric study are summarized below:

- The presence of thermal dispersion plays a significant role in the modification temperature field and heat transfer rate.
- The homogeneous and heterogeneous reactions parameters cause a decrease in the species concentration and the rate of mass transfer at the plate.
- The presence of porous medium parameter leads to decrease the velocity near the plate and the local Nusselt Number.
- The presence of hybrid nanoparticles in working fluid enhance the both of skin friction coefficient and the heat transfer rate.
- The changing in the stretching parameter leads to improve the dynamic behavior and the heat transport near the sheet.

ORCID

Zohra Terbiche, https://orcid.org/0009-0000-5241-326X; **Hamza Ali Agha,** https://orcid.org/0009-0002-2152-886X
Soufiane Rahal, https://orcid.org/0000-0002-3252-8921; **Nadir Boutalbi,** https://orcid.org/0009-0000-0382-5671

REFERENCES

[1] K. Khanafer and K. Vafai, J. Therm. Anal. Calorim. **135**, 1479 (2019). https://doi.org/10.1007/s10973-018-7565-4
[2] K. Vafai, *Handbook of porous media*, third Ed., (CRC Press, New York, 2015). https://doi.org/10.1201/b18614
[3] Y. Mahmoudi, K. Hooman and K. Vafai, *Convective Heat Transfer in Porous Media*, first Ed., (CRC Press, New York, 2019). https://doi.org/10.1201/9780429020261
[4] D.A. Nield and A. Bejan, *Convection in Porous Media*, fifth Ed., (Springer, New York, 2017). https://doi.org/10.1007/978-3-319-49562-0
[5] C. Sowmiya and B.R. Kumar, Therm. Sci. Eng. Prog. **53**, 102772 (2024). https://doi.org/10.1016/j.tsep.2024.102772
[6] S. Khalil, T. Abbas and R. Nawaz, Nano-Struct. Nano-Objects, **40**, 101350 (2024). https://doi.org/10.1016/j.nanoso.2024.101350
[7] D. Pal, and G. Mandal, J. Pet. Sci. Eng. **126**, 16 (2015). https://doi.org/10.1016/j.petrol.2014.12.006.
[8] J.A. Adigun, A. Adeniyan and I.O. Abial, Int. Commun. Heat Mass Transfer, **126**, 105479 (2021). https://doi.org/10.1016/j.icheatmasstransfer.2021.105479
[9] S. Nandi, B. Kumbhakar, and S. Sarkar, Int. Commun. Heat Mass Transfer, **130**, 105791 (2022). https://doi.org/10.1016/j.icheatmasstransfer.2021.105791
[10] K.K. Asogwa, B.S. Goud, Y.D. Reddy and A.A. Ibe, Results Eng. **15**, 100518 (2022). https://doi.org/10.1016/j.rineng.2022.100518
[11] P.K. Kameswaran, P. Sibanda, Bound. Value Probl. 2013 (2013) 1-12. https://doi.org/10.1186/1687-2770-2013-243.
[12] A.M. Bouaziz, S. Hanini, J. Mech. 32 (2016) 441 – 451. https://doi.org/10.1017/jmech.2016.18.
[13] M.A. Sheremet, I. Pop, and N. Bachok, Int. J. Heat Mass Transfer **92**, 1053 (2016). https://doi.org/10.1016/j.ijheatmasstransfer.2015.09.071
[14] Ch. RamReddy and Ch. Venkata Rao, Nonlinear Eng. **6**, 277 (2017). https://doi.org/10.1515/nleng-2016-0071
[15] P. Sudhagar, P.K. Kameswaran, and B.R. Kumar, J. Porous Media, **23**, 923 (2020). https://doi.org/10.1615/JPorMedia.2020024874
[16] F.G. Awad, P. Sibanda and P.V.S.N. Murthy, ASME J. Heat Mass Transfer, **137**, 104501 (2015). https://doi.org/10.1115/1.4024895
[17] Om P. Meena, P. Janapatla and G. Kumar, Appl. Math. Comput. **430**, 127072 (2022). https://doi.org/10.1016/j.amc.2022.127072
[18] N.S. Khashi'ie, N.Md. Arifin, and I. Pop, Int. Commun. Heat Mass Transfer, **118**, 104866 (2020). https://doi.org/10.1016/j.icheatmasstransfer.2020.104866
[19] X. Song, L.D. Schmidt and R. Aris, Chem. Eng. Sci. **46**, 1203 (1991). https://doi.org/10.1016/0009-2509(91)85049-4
[20] M.A. Chaudhary, and J.H. Merkin, Fluid Dyn. Res. **16**, 311 (1995). https://doi.org/10.1016/01695983(95)00015-6
[21] J.H. Merkin, Math. Comput. Model. Dyn. **24**, 125 (1996). https://doi.org/10.1016/08957177(96)00145-8
[22] F. Alzahrani, R.J.P. Gowda, R.N. Kumar, and M.I. Khan, J. Indian Chem. Soc. **99**, 100458 (2022). https://doi.org/10.1016/j.jics.2022.100458
[23] Ch. Liu, M. Pan, L. Zheng and P. Lin, Int. Commun. Heat Mass Transfer, **110**, 104434 (2020). https://doi.org/10.1016/j.icheatmasstransfer.2019.104434
[24] S. Bashir, I.M. Almanjahie, M. Ramzan, A.N. Cheema, M. Akhtar and F. Alshahrani, Heliyon, **10**, e24718 (2024). https://doi.org/10.1016/j.heliyon.2024.e24718
[25] M. Irfan, M. Khan and W.A. Khan, J. Braz. Soc. Mech. Sci. Eng. **41**, 135 (2019). https://doi.org/10.1007/s40430-019-1619-9

[26] P. Sunthrayuth, S.A. Abdelmohsen, M.B. Rekha, K.R. Raghunatha, A.M. Abdelbacki, M.R. Gorji and B.C. Prasannakumara, Case Stud. Therm. Eng. **32**, 32101897 (2022). https://doi.org/10.1016/j.csite.2022.101897
[27] Z. Abbas and M. Sheikh, Chin. J. Chem. Eng. **25**, 11 (2017). https://doi.org/10.1016/j.cjche.2016.05.019
[28] T. Hayat, M.I. Khan, A. Alsaedi and M.I. Khan, J. Mol. Liq. **223**, 960 (2016). https://doi.org/10.1016/j.molliq.2016.09.019
[29] O. Plumb, in: *Proc. First ASME/JSME Thermal Engineering Joint Conference 2*, (Honolulu, HI, USA, 1983), pp. 17–21.
[30] J.T. Hong and C.L. Tien, Int. J. Heat Mass Transfer, **30**, 143 (1987). https://doi.org/10.1016/0017-9310(87)90067-6
[31] S. Yagi, D. Kunii and K. Endo, Int. J. Heat Mass Transfer, **7**, 333 (1964). https://doi.org/10.1016/0017-9310(64)90109-7
[32] J.R. Babu, K.K. Kumar and S.S. Rao, Renewable Sustainable Energy Rev. **77**, 551 (2017). https://doi.org/10.1016/j.rser.2017.04.040
[33] B. Takabi and S. Salehi, Adv. Mech. Eng. **6**, 147059 (2014). https://doi.org/10.1155/2014/147059
[34] H.F. Oztop and E. Abu-Nada, Int. J. Heat Fluid Flow, **29**, 1326 (2008). https://doi.org/10.1016/j.ijheatfluidflow.2008.04.009
[35] H. Ali Agha, M.N. Bouaziz and S. Hanini, J. Mech. **31**, 607 (2015). https://doi.org/10.1017/jmech.2015.28
[36] M. Hussain, A. Ali, S.W. Yao, A. Ghaffar, and M. Inc, Case Stud. Therm. Eng. **31**, 101809 (2022). https://doi.org/10.1016/j.csite.2022.101809
[37] L. Shampine, I. Gladwell, and S. Thompson, *Solving ODEs with matlab*, first Ed., (Cambridge University Press, United Kingdom, 2003). https://doi.org/10.1017/S0025557200178088
[38] N. Bachok, A. Ishak and I. Pop, Nanoscale Res. Lett. **6**, 623 (2011). https://doi.org/10.1186/1556-276X-6-623
[39] R. Nandkeolyar, S.S. Motsa and P. Sibanda, J. Nanotechnol. Eng. Med. **4**, 041002 (2013). https://doi.org/10.1115/1.4027435
[40] N.A. Yacob, A. Ishak and I. Pop, Int. J. Thermal. Sci. **50**, 133 (2011). https://doi.org/10.1016/j.ijthermalsci.2010.10.008
[41] P.K. Kameswaran, S. Shaw, P. Sibanda and P.V.S.N. Murthy, Int. J. Heat Mass Transfer, **57**, 465 (2013). https://doi.org/10.1016/j.ijheatmasstransfer.2012.10.047

ВПЛИВ КОМБІНОВАНИХ ХІМІЧНИХ РЕАКЦІЙ ТА ТЕПЛОВОЇ ДИСПЕРСІЇ НА КОНВЕКТИВНИЙ ПОТІК У ПОРИСТОМУ СЕРЕДОВИЩІ З ГІБРИДНОЮ НАНОРІДИНОЮ

Зохра Тербіше[a], Хамза Алі Ага[a,b], Суфіан Рахал[a], Надір Бутальбі[b]

[a]*Лабораторія біоматеріалів та явищ переносу (LBMPT), Технологічний факультет, Університет Яхія Фарес Медейський, Поле Урбен Медейський, 26000, Алжир*

[b]*Лабораторія механіки, матеріалів та енергетики (L2ME), Технологічний факультет, Університет А. МІРА з Беджаї, Таргуа Узмур Беджая, 06000, Алжир*

Це дослідження характеризується чисельним аналізом впливу теплової дисперсії на потік тепло- та масопереносу до розтягуваної пластини в насиченому пористому середовищі, заповненому гібридною нанорідиною Cu/Al2O3-вода, враховуючи наявність гомогенних (НОМ)-гетерогенних (НЕТ) хімічних реакцій. Побудовано нову модель хімічних реакцій (НОМ-НЕТ), де реакції (НЕТ) відбуваються на поверхнях твердої матриці в пористому середовищі та пластині, дотримуючись кінетики першого порядку. На відміну від цього, гомогенна реакція (НОМ) відбувається в рідкій фазі та описується ізотермічною кубічною автокаталітичною кінетикою. Явища імпульсу, енергії та масопереносу визначаються набором диференціальних рівнянь з частинними похідними з відповідними перетвореннями подібності, які дають чотири зв'язані нелінійні звичайні диференціальні рівняння. Отримана система рівнянь, що визначає, розв'язується чисельно за допомогою обчислювально ефективної схеми скінченних різниць. Числові результати перевірено шляхом порівняння з наявними даними, що показує хорошу узгодженість. Числові результати демонструють вплив фізичних параметрів керування на динаміку потоку, розподіл тепла та профілі концентрації розчинених речовин. Крім того, ключові характеристики розчину, включаючи число Нуссельта та коефіцієнт тертя поверхні, зведені в таблиці.

Ключові слова: *гібридна нанорідина; термічна дисперсія; потік у точці застою; пористе середовище*